

Balance of pH and Ionic Strength Influences on Chain Melting Transition in Catanionic Vesicles

Claire Vautrin,^{*,†} Thomas Zemb,[†] Matthias Schneider,[‡] and Motomu Tanaka[‡]

Service de Chimie Moléculaire, CEA Saclay, 91191 Gif-sur-Yvette, France, and Lehrstuhl für Biophysik E22, Technische Universität München, D-85748 Garching, Germany

Received: December 10, 2003; In Final Form: March 23, 2004

We study the thermotropic phase transition of “salt-free” mixtures of single-tailed cationic and anionic surfactants, called “catanionic systems” in this paper, for concentrated (10 wt %) and diluted (0.5 wt %) samples. Small-angle neutron scattering (SANS) and differential scanning calorimetry (DSC) demonstrate that the chain melting phase transition is identical for diluted and concentrated samples at the same mole fraction (r) of anionic surfactants. The addition of anionic surfactants (for $r = 0.5$ – 0.7) induces an increase of the global surface charge, followed by an increase of the main transition temperature. This evolution may be interpreted as the hydrogen bonding formation between carboxylic acid headgroups. At $r \sim 0.6$, corresponding to the region where faceted vesicles are formed, the “melting” of the alkyl chains is a progressive process extending over 15 °C. Here, molten and crystallized bilayers coexist in swollen lamellar phases of catanionic bilayers. This coexistence explains the increase of the viscosity of the solution, via structural reorganization of the bilayers or friction between the partially fused vesicles.

Introduction

Mixtures of single-tailed cationic and anionic surfactants (catanionics) are known to produce a very rich range of aggregate microstructures and, in particular, present simultaneously low spontaneous curvature due to ion-pair forming.^{1,2} In the absence of additional salt, catanionic bilayers are expected theoretically to show high bending rigidity.³ This rigidity of salt-free catanionics has been shown by observation of a very limited binding by cryoelectron microscopy.⁴

Since such aggregates are formed by electrostatic interactions between the two oppositely charged headgroups, it is necessary to study so-called “salt-free” (also called “true”) catanionics. Here, influence of counterions still dominates, and therefore it is possible to compensate the free energy associated with local segregation of the components.⁵ Salt-free catanionics were studied first by Bengt Jönsson and P. Jokela,^{6–9} reporting a limited swelling of lamellar phases without charge at equimolar ratio. However, they observed an increase in the swelling at nonequimolar ratio, which can only be explained by coexistence of small, crystallized colloids in lamellar phases.⁴

Highly charged aggregates can be prepared by mixing the corresponding acid and hydroxide surfactants without counterions, so no excess salt is formed.¹⁰ In such ternary systems, two variables control the molecular interactions: the weight fraction Φ of surfactants and the molar ratio r of anionic surfactant ($r = n_{\text{acid}}/n_{\text{acid}} + n_{\text{base}}$). For such “rigid” systems with a two-dimensional network of opposite charges, it is therefore interesting to study the influence of surface net charges on the thermotropic phase transition (e.g., chain melting) as a function of pH of the solution, since changing pH after formation of the aggregate will change the surface effective charge. The role of charge screening has been described in the literature for classical catanionic systems,¹¹ as well as pH and ionic strength effects

on phospholipid systems,^{12–14} and more recently on catanionic vesicles.¹⁵ The first step in this direction is to determine if chain melting transitions are identical for the concentrated and diluted phases present in the phase diagram.

Following our recent calorimetry experiments on phase behavior of concentrated, swollen lamellae ($\Phi = 10$ wt %),^{16,17} we study here the thermotropic phase transition of salt-free catanionics of myristic acid and cetyltrimethylammonium hydroxide in diluted phases ($\Phi = 0.5$ wt %), which form polyhedral-shaped vesicles.¹⁸

Materials and Methods

The cationic surfactant cetyltrimethylammonium hydroxide (CTAOH) was prepared by ion exchange (resin Bio-Rad 100-200 Mesh) with a basic ion exchanger from the bromide salt, purchased from Fluka (Germany) and used without further purification. The quality of the ion exchange was checked by electrophoresis with a Waters capillary ion analyzer. The quantity of residual bromide counterions was evaluated to be 2.2 mol %. Tetradecanoic acid (myristic acid, abbreviated as C13COOH) was purchased from Fluka and used after recrystallization in acetonitrile. The composition of the samples is given by the molar ratio of C13COOH to total surfactant concentration (r), and the total surfactant concentration (Φ) in weight percent.

Heat capacity profiles were recorded on a Microcal MC2 calorimeter (Northampton, MA) by using a scan rate of 15 °C/h. The resolution of this instrument was proven to be around 0.15 μW with a standard deviation of 0.025 μW .¹⁹ The cell volume was fixed to 0.5 mL. To confirm the equilibration, two successive heating/cooling cycles repeated. The obtained heat capacity scans were analyzed using the routine of the Origin software. Viscosity measurements have been performed with a Couette geometry rheometer (Rheometrix RFS2) with a gap of 0.25 mm (6.28 rad s⁻¹, 50% deformation). ζ -Potentials of the vesicle suspensions were determined by measuring the electrophoretic mobility using a Zetameter Coulter Delsa 440SX. The

* Corresponding author. E-mail: vautrin@scm.saclay.cea.fr.

[†] CEA Saclay.

[‡] Technische Universität München.

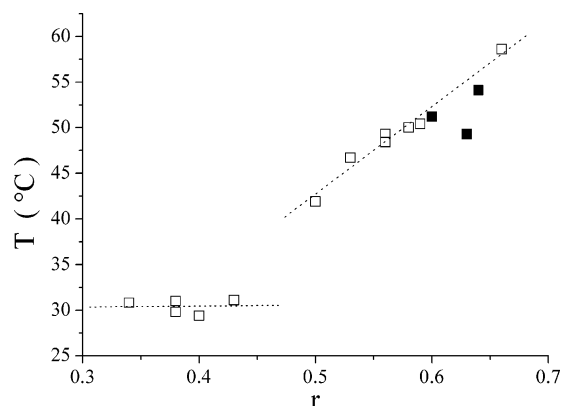


Figure 1. Main chain melting temperature T_m as a function of molar ratio of myristic acid r . T_m is almost constant in the presence of excess CTAOH ($r < 0.45$), whereas it remarkably increases at $r > 0.50$. The open symbols stand for concentrated samples ($\Phi = 10$ wt %), and the closed symbols stand for diluted ones ($\Phi = 0.5$ wt %).

apparatus uses the laser-Doppler effect to measure the electrophoretic mobility.

Small-angle neutron scattering (SANS) measurements were carried out at the PAXE beam line of the LLB (Laboratoire Léon Brillouin, Saclay, France) equipped with a two-dimensional detector. The incident wavelength used here was $\lambda = 5$ Å. The measured q -range had to be extended up to $q = 0.42$ Å⁻¹, obtaining a spatial resolution down to $\pi/q_{\max} = 1.2$ nm. This enables one to determine the bilayer thickness from the high angle minima in the scattering function without absolute scale measurements.²⁰

Results

Comparison of Concentrated and Diluted Catanionics.

Figure 1 shows the positions of the main endothermic peak plotted as a function of molar ratio r . The phase transition temperatures for concentrated ($\Phi \sim 10$ wt %) and diluted ($\Phi \sim 0.05$ wt %) samples were measured by differential scanning calorimetry (DSC). As presented in the figure, two regimes could be observed.

With an excess of cationic CTAOH ($0.3 < r < 0.5$), the chain melting temperature is almost constant. SANS measurements of a concentrated sample (e.g., $\Phi \sim 19$ wt %) yield a lamellar periodicity of $D^* = 135$ Å, suggesting that the alkyl chains are interdigitated. In fact, by assuming the conservation of volume, the bilayer thickness (d) can be estimated to be $d = D^*$. $\Phi = 25$ Å, which is reasonable for that of interdigitated chains.¹⁶ This interdigitation is attributed to the electrostatic repulsion between the positively charged ammonium headgroups. The transition temperature is mainly dependent on the hydrophobic interaction, rather than the r value.

On the other hand, an excess of anionic C13COOH ($0.5 < r < 0.7$) increases the chain melting temperature because of the enhanced in-plane correlation via hydrogen bonds between acid dimers called “acid soaps”.^{21,22} When dissolving a pure carboxylic acid RCOOH in sodium hydroxide solution, a fine precipitate of acid soap (RCOO)₂HNa is formed. In our case, the carboxylic acid C13COOH is dissolved not in sodium hydroxide solution but in CTAOH solution. There is no sodium to neutralize the myristate–myristic acid crystallizing together (acid soap), but there are ammonium headgroups CTA⁺. In this domain, the transition temperature is dependent on the head-group interactions and, as a result, increases with the number of hydrogen bonds between headgroups.

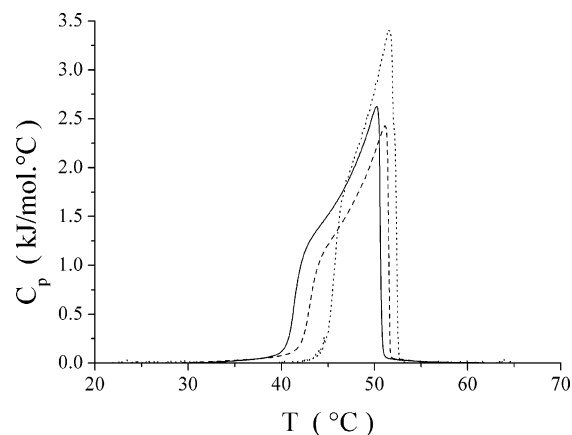


Figure 2. DSC scans of samples with $r = 0.6$. Dotted, solid, and dashed lines correspond respectively to $\Phi = 0.05$, 1.7, and 5.0 wt %. The global shape, the peak position, and the transition enthalpy are almost identical for diluted and concentrated samples.

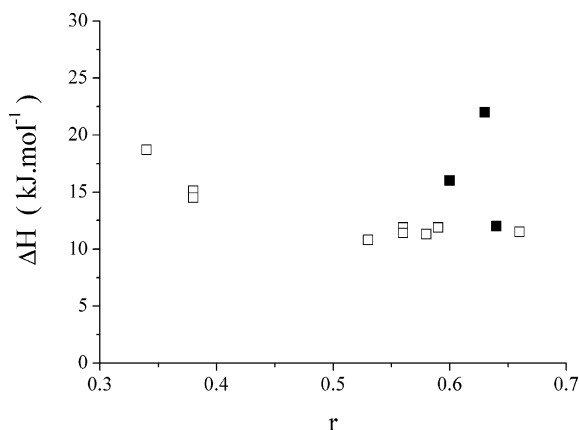


Figure 3. Calculated phase transition enthalpy ΔH plotted as a function of molar ratio r , yielding the mean value of 15 ± 5 kJ mol⁻¹. The open symbols correspond to the concentrated samples ($\Phi = 10$ wt %), while the closed symbols correspond to the diluted ones ($\Phi = 0.5$ wt %).

For diluted samples, the available molar fraction of C13COOH is limited at $r \sim 0.6$, corresponding to the region where faceted vesicles are formed. At $r < 0.5$, the monophasic domain is too diluted for DSC analyses, while the samples become biphasic at $r > 0.7$ as myristic acid is poorly soluble in water. The DSC scans of the catanionic samples with $\Phi = 0.05$, 0.19, and 5 wt % are shown in Figure 2, where the main transition peak seems to be almost independent of the total surfactant concentration Φ . One broad chain melting transition can be observed at 52 °C, whose width ranges up to 10 °C.

Here, the phase transition enthalpy can be determined by integration of the whole curves, yielding similar values of 15 ± 5 kJ mol⁻¹, independent of the total surfactant concentration.

If we compare the value obtained for the phase transition enthalpy ($15 \times 2 = 30$ kJ·mol⁻¹) with the corresponding values of double-chain phospholipids, there is good agreement with the corresponding values of double-chain phospholipid with cetyl and myristoyl chains,²³ 28.5–34 kJ·mol⁻¹. Thus, the phase transition of catanionics here seems to be dominated by hydrophobic interaction between the alkyl chains.

“Progressive” Chain Melting of Faceted Vesicles. Figure 4a–c presents the SANS scans of catanionic vesicles ($\Phi = 0.1$ wt %, $r = 0.6$) measured at three different temperatures, below (25 °C, a), above (66 °C, c), and in the vicinity (47 °C, b) of the phase transition. As a reference, the DSC scan of the same sample is given in the upper panel.

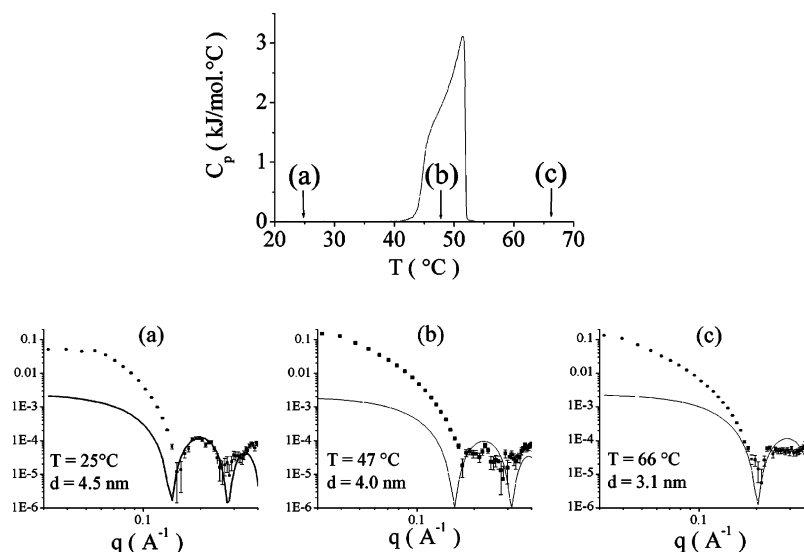


Figure 4. SANS scans of catanionic vesicles ($\Phi = 0.1$ wt %, $r = 0.60$), measured at 25, 47, and 66 °C. Solid lines correspond to the simulated form factors, yielding average thickness d of 45, 40, and 31 Å, respectively. The DSC scan of the same sample is given in the top panel as a reference.

The lamella thickness was deduced from the experimental results: the form factor of an infinite plane with the thickness of d , $P(q) = K(\sin(qd/2)/q)^2$, was taken, because the mean radius of the vesicles¹⁸ ($R \sim 2 \mu\text{m}$) is large enough to be neglected. This form factor presents a first sharp zero at $q = \pi/d$, yielding the average thickness d .

We found out that the average thickness of the bilayer is 45 Å at 25 °C, 40 Å at 47 °C, and 31 Å at 66 °C. In comparison to the bilayer thickness below the transition temperature (25 °C), the bilayer thickness decreased by 10% at the middle of the transition (47 °C). Across the phase transition, the bilayer thickness decreased by 30% (66 °C), which is reasonable compared to that of the disordered alkyl chains. In the vicinity of the phase transition (47 °C), the fit of the experimental curve shows a relatively large error (± 2 Å), suggesting the coexistence of disordered and ordered chains. Such phase coexistence in a wide temperature range (in the present case, almost 10 °C) is clearly different from the first-order phase transition of conventional phospholipids, indicating that the observed phase transition is rather progressive. In fact, our previous wide-angle X-ray scattering (WAXS) experiments on the concentrated sample¹⁶ ($\Phi = 10$ wt %, $r = 0.6$) revealed that the chain correlation peak q_{100} at $q = 1.54 \text{ Å}^{-1}$ remained sharp and intense across the phase transition. Thus, we concluded that the chain melting transition of faceted vesicles is also progressive. In fact, the coexistence of ordered and disordered chains has already been observed even in “single-component” vesicles.^{24,25} It should be noted that such a phase coexistence is not due to the fact that single-walled vesicles are not always the true thermodynamic equilibrium, nor is it due to a finite size effect^{26,27} as each vesicle studied here contains approximately 2×10^7 molecules (estimated from the average size of a vesicle). The broadening of the capacity curve can be explained by assuming a nonideal mixture between the components. The mixture would then present a solid–liquid miscibility gap. For example, Blume and co-workers²⁸ applied this model to phospholipid mixtures and Dörfler²⁹ to lipid–phospholipid systems.

Influence of the Membrane Surface Charges. As we previously reported,¹⁸ faceted vesicles can be formed only at around $r = 0.6$ in diluted suspensions ($\Phi < 1.5$ wt %); we changed the surface charge of catanionic vesicles ($r = 0.6$, $\Phi = 0.2$ wt %) by titration of pH with HCl. Figure 5 shows the

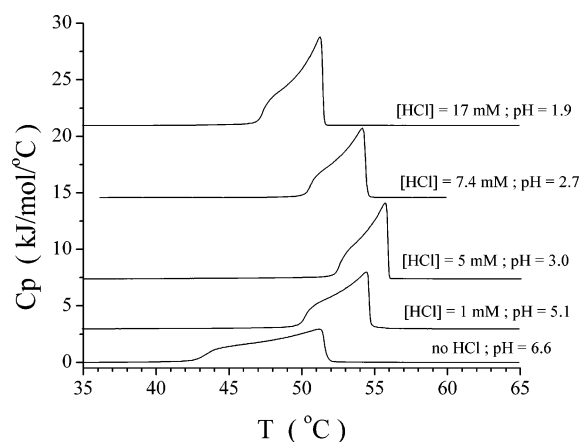


Figure 5. Heat capacity scans of catanionic vesicle suspensions ($\Phi = 0.2$ wt %, $r = 0.60$) at pH 6.6–1.9. The final concentration of HCl is given to roughly estimate the ionic strength of each sample.

DSC scans of the catanionic vesicles at pH 6.6 (as prepared), 5.1, 3.0, 2.7, and 1.9.

The global shape of the DSC scan and the position of the transition temperature are dependent on acid addition, but the transition enthalpy remains constant, $\Delta H = 16$ kJ/mol. A continuous increase in the transition temperature from 52 to 56 °C was observed according to the pH titration from 6.6 to 3.0. The transition peak became sharper, while the width of the transition regime decreased from 10 to 4 °C. On the contrary, further titration with HCl to pH 1.9 resulted in the decrease in the transition temperature to 52 °C, followed by the broadening of the transition regime.

To relate evolution of the phase transition temperature and enthalpy in accordance with the effective surface charges, we performed electrophoretic mobility measurements of catanionic vesicles ($\Phi = 0.2$ wt %, $r = 0.60$) to determine ζ -potentials of the membrane surface (Figure 6). Vesicles are large enough (mean diameter of $2 \mu\text{m}$) that the electrophoretic mobility can be linked to the ζ -potential by the Smoluchowski equation $\zeta = \eta u / \epsilon$. Here, ϵ is the dielectric constant, η is the viscosity of the solvent, and u is the mobility of the particles.

The first interesting finding is the measured sign of the vesicle charge.³⁰ At $r = 0.6$, as-prepared vesicles seem to be positively charged, where the obtained mobility of $3 \pm 1 \mu\text{m cm}/(\text{V s})$

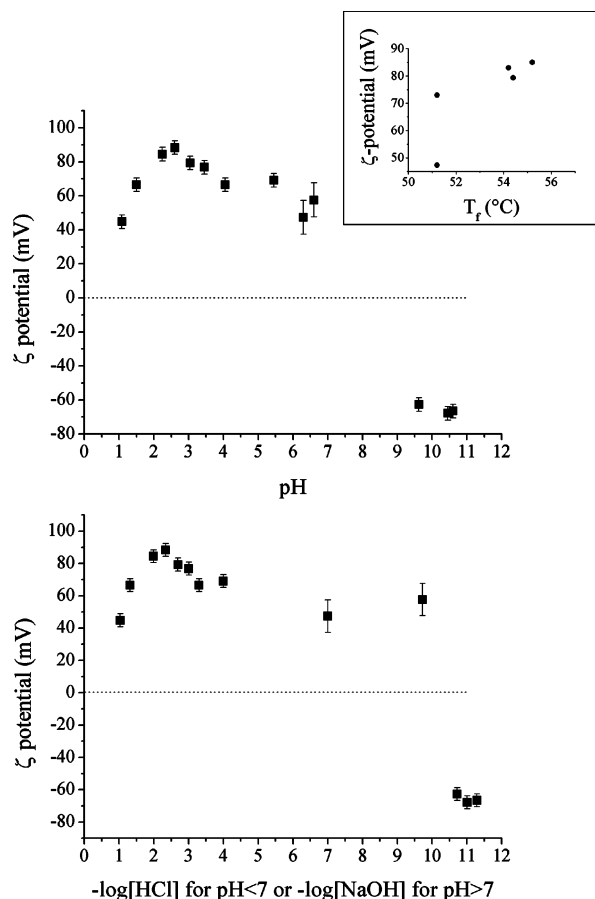


Figure 6. Influence of pH on surface potential of catanionic vesicles ($\Phi = 0.2$ wt %, $r = 0.60$). (top) Classical representation; (bottom) representation as a function of acid/base concentration; (inset) plot of transition temperature from Figure 3 versus ζ -potential to illustrate the relationship between the surface charge and the transition temperature.

leads to a surface charge density of 10^{-24} C \AA^{-2} (i.e., $0.01 \mu\text{C cm}^{-2}$) by assuming the Smoluchovsky model. The association of CTAOH and C13COOH produces $\text{CTA}^+\text{C13COO}^-$ ion pairs until almost no free CTA^+ remains. The positive ζ -potential observed around pH 7 (~ 50 mV, Figure 6, top) suggests that the excess of myristic acids are protonated and form dimers.

Such cocrystallization of myristic acid and the sodium salt is called “acid soap”.^{21,22} Infrared measurements of Mantsch et al.³¹ demonstrated that the C–O vibrations in acid soaps can be divided into three different bands: “dissociated” carboxyl groups have a maximum at 1550 cm^{-1} ; “protonated” ones have a maximum at $1700\text{--}1720 \text{ cm}^{-1}$. The protonated carboxyl group bound to a neighboring carboxyl group via hydrogen bonding has an absorption at 1650 cm^{-1} .

Here, the presence of hydrogen bonding between adjacent carboxyl groups may explain the surprising relationship between the phase transition temperature and the ζ -potential (inset, Figure 6): the transition temperature increases according to the increase in the number of hydrogen bonds between adjacent carboxyl groups.

From the results presented in Figure 6, we can distinguish four regimes where the catanionics react differently to the pH titration:

(1) When the concentrations of HCl and NaOH added for titration are below 0.1 mM (i.e., at pH $\sim 6\text{--}8$), the screening length κ^{-1} was above 300 \AA . Here, the ζ -potential is quite stable around 50 mV .

(2) When pH drops below pK_a of about 5, the ratio of protonated to deprotonated carboxylate headgroups strongly

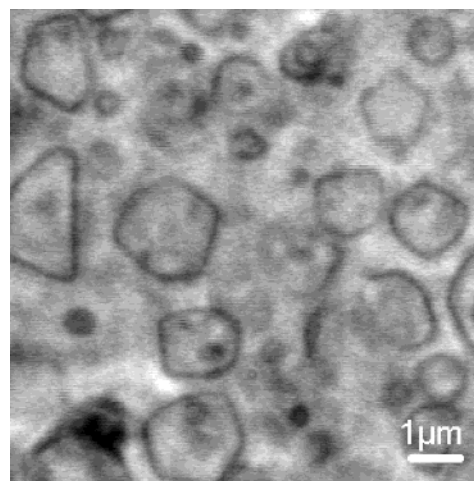


Figure 7. Phase contrast micrograph of faceted vesicles ($\Phi = 0.25$ wt %, $r = 0.60$), titrated with 5 mM HCl at 25°C .

increases. The titration of pH from 5 to 2.5 leads to a decrease in the number of ion pairs $\text{CTA}^+\text{C13COO}^-$ on behalf of the number of dimers $\text{C13COOH}\text{C13COO}^-$, which results in the clear increase in the ζ -potential.

(3) If HCl concentration exceeds 5 mM (i.e., pH < 2.5), the screening length κ^{-1} is smaller than 40 \AA . Here, the ionic strength becomes the dominant parameter. The electrostatic interaction between the headgroups is screened; namely, acid is less dissociated and the electrical double layer is dissipated near the surface. The chloride ions are closer to the surface, explaining the decrease in the ζ -potential.

(4) The last domain (pH > 7), where NaOH concentration is more than 1 mM , has been less studied by DSC because the samples were metastable to gain reproducible results. In this domain, the ammonium headgroups associate with hydroxide ions, and therefore, the dissociation rate of carboxylic acid increases. Thus, global charge of the vesicles becomes negative under these conditions.

Over the whole pH range explored in this study, the vesicles were never “highly charged” because the dissociation rate still remains low. Since the background salt is only about 10^{-5} M , the ζ -potential values are always below 100 mV . Assuming a polar area per crystallized surfactant of 20 \AA^2 , there should be around one dissociated surfactant per 1000 surfactants. This means that the ratio of the “effective charge” to the “structural charge” was always less than 1% . To support the above-mentioned hypotheses, we further confirmed that the addition of HCl does not influence the mean size of the vesicles by phase contrast microscopy (Figure 7).

Viscosity of Catanionic Vesicles at Phase Coexistence.

Another interesting point is that an increase in the ionic strength reduces the width of the phase transition. As shown in Figure 8, we observed that the changes in viscosity of catanionic vesicles ($\Phi = 0.1 \text{ wt } \%, r = 0.60$) exactly follow the heat capacity changes. In the transition region, there is a strong increase in the viscosity at the phase coexistence, in contrast to low viscosity at low and high temperature phases.

In fact, the peak position in DSC scans coincides with the viscosity maximum. Moreover, the viscosity of the vesicle suspension in the high temperature state is less than that of the low temperature phase, possibly due to a reduction in mean diameter of the vesicles upon progressive chain melting. We further tried to relate the chain melting transition to the transition in viscosity for samples in the presence of additional HCl. However, it appeared to be practically difficult because the

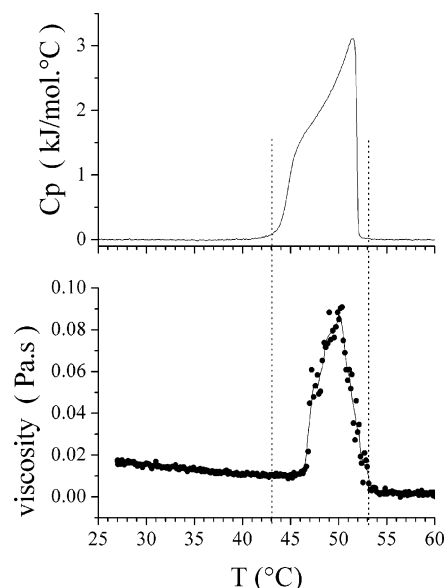


Figure 8. Heat capacity scan (top) and viscosity (bottom, measured at 6.28 rad s⁻¹, 50% deformation) of catanionic vesicles ($\Phi = 0.1$ wt %, $r = 0.60$). The line in the viscosity plot is given to guide the eye.

increase in HCl concentration reduced the width of the endothermic phase transition as well as that of the mechanical transition, which seems qualitatively similar to previous reports on DMPG vesicles.³²

Discussion

In phospholipid membranes with charged lipids, an increase of the chain melting temperature can be explained in terms of either (i) a decrease in the ionization state of the polar headgroups, (ii) a screening of the electrostatic repulsion by high ionic strength, or (iii) an increase in the lipid–lipid hydrophobic attraction following a decrease in the polar head hydration.¹⁴

In the case of catanionics, these three arguments have to be invoked simultaneously to explain our experimental findings. In the first two regimes (pH 2.5–6.6) with low ionic strength ($[HCl] < 5$ mM), the phase transition temperature (Figure 5) as well as the ζ -potential (Figure 6) increases with the addition of HCl. Here, the total energy gain from the hydrogen bonding between protonated and deprotonated headgroups is larger than the energy loss due to the electrostatic repulsion between charged ammonium headgroups. In the third regime, the ionic strength is the dominant parameter. Here, the screening of the electrostatic repulsion between ammonium groups is overcome by a screening of the electrostatic attraction between carboxylate and ammonium groups, resulting in a decrease in T_m .

One of the possible scenarios to understand the observed correlation between ΔC_p and $\Delta\eta$ is the phase transition resulting from the increase in lateral membrane compressibility.³² If one assumes the influence of the membrane compressibility on the phase transition,³³ the broad peaks observed in the heat capacity scans can be interpreted as the phase transitions of the membranes with different curvatures and topologies. Such transitions have previously been reported for locally flat bilayers without long-range structural order, such as sponges, asymmetric sponges, and vesicles.³⁴ These transitions are strongly influenced by the headgroup–solvent interactions ΔG_{sol} , which are dependent upon membrane curvatures and topologies.³⁵ Thus, it is reasonable that the salt concentration and the pH can change the width of mechanical and thermotropic phase transitions of

the catanionics. As the surface charge density (ζ -potential) increases, the free energies of the phases with different topologies are getting closer, resulting in the narrower phase transition regime. On the contrary, a decrease in surface charge density (ζ -potential) is expected to cause the opposite effect, which could be observed actually in our experiments (Figures 5 and 6). Thus, the pronounced change in viscosity as well as the extended phase transition regime can be understood within this framework.³²

In the intermediate regime, the viscosity of dispersions showed increases almost by a factor of 5, whereas the lamellar thickness is close to that of a bilayer in gel phase. One of the possibilities could be a kind of $P_{\beta'}$ phase, which includes disordered chains within ordered chains.³⁵ The capacity profile could also result from a two-step mechanism: first, the headgroups dissociate without any change in the membrane thickness and, second, the chains melt inducing an increase of the thickness. These two steps have been described previously by other groups using SANS³⁶ or FTIR.³¹ Moreover, Döbereiner and co-workers^{37,38} postulated that the phase transition of DMPG vesicles is influenced by the surface charge densities.

In macroscopic scale, we concluded that the thermotropic phase transition of catanionic vesicles is progressive, which typically ranges over 10–15 °C. By considering one closed thermodynamic system, there are only two detectable packing modes of chains: “ordered” and “disordered”. We know that for any volume ratio an infinite lattice does not exist. Indeed, it is expected, following the Kosterlitz–Halperin–Thouless theory of frustrated melting in a plane,³⁹ that the transition is slightly second order from a thermodynamic point of view. However, from the width of the SAXS Bragg peak,¹⁷ we expect the order to propagate over 10^4 chains and the corresponding broadening of the melting to be $\sim 10^{-2}$ K. On a microscopic scale, the transition occurring there must be a first-order transition. However, if one considers an assembly of vesicles with a variety of curvatures and topologies, progressive melting versus temperature is compatible with the heat capacities observed by DSC. Here, bilayers that are locally flat in the length scale of ξ (corresponding to the in-plane coherence length) can be dispersed without long-range order, e.g., a smectic liquid crystalline phase. If we look at Figure 7, we can see that the in-plane coherence length for the catanionics is around 1 μm . There are three classes of those random dispersions of the bilayers: a (symmetric) sponge phase, an asymmetric sponge phase, and a dispersion of vesicles. These three microstructures differ only by one order parameter (usually ψ), which can be seen as the ratio of volume situated inside (or left of) and outside (or right of) bilayers.^{34,40} In the catanionic vesicles studied here, we have Φ of about 0.1 wt %. From $\psi/\Phi \sim R/d$, one can calculate $\psi \sim 0.25$, which is above the percolation threshold ($\psi \sim 0.12$). Therefore, if the vesicle dispersion is partially molten, there are three possible intermediate states between ordered and disordered states as represented in Figure 9. Viscosity can follow the “melting” of the alkyl chains, if (i) some faces of an asymmetric sponge phase bridge adjacent partially molten objects (upper line), or (ii) an asymmetric sponge phase melts on some faces, thus common to neighboring polyhedra as in a biliquid foam (middle line).^{40,41} The bottom line describes cooperative melting, which cannot explain a maximum in the viscosity.

Döbereiner suggested scheme (i) by so-called flicker microscopy^{37,38} for DMPG vesicles in the presence of divalent cation impurities. They related high viscosity observed during the transition to the friction between partially fused vesicles, relying

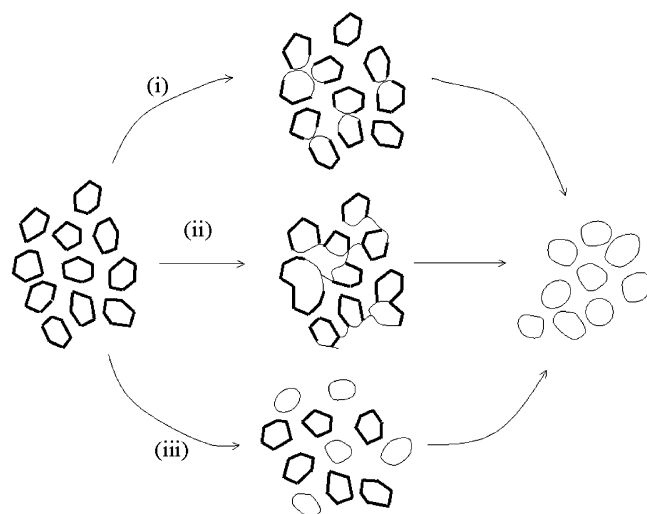


Figure 9. Three possible intermediate states between faceted (crystallized) polyhedra and vesicles. The thick lines symbolize the ordered chains, while the fine, curved lines stand for the disordered chains. The intermediate states correspond to the phase transition regime where the maxima in C_p and viscosity occur.

on the interactions between ordered and disordered bilayers. On the other hand, Schneider et al.³² have proposed scheme (ii) for DMPG vesicle suspension using freeze–fracture electron microscopy, explaining the high viscosity at the intermediate phase in terms of structural reorganization of vesicles under equilibrium with lamellar phases.

The high viscosity observed during the transition, according to the first mechanism, is related to friction between partially fused vesicles, while the viscosity in the second mechanism is related to structural reorganization of vesicles in equilibrium with lamellar phases. The first mechanism relies on interactions between the molten and crystallized bilayers, while this reorganization of secondary structure along the latter scenario requires a variation of average curvature.

Acknowledgment. M.S. and M.T. thank E. Sackmann for helpful discussion, and M.T. is thankful to DFG for the habilitation fellowship (Emmy Noether Program, Phase II). This work has financially been supported by CNRS and DFG through the French–German network “Complex fluids in two and one half dimensions”.

References and Notes

- (1) Kaler, E. W.; Herrington, K.; Kamalakara Murthy, A.; Zasadzinski, J. *J. Phys. Chem.* **1992**, *96*, 6698.
- (2) Kaler, E. W.; Kamalakara Murthy, A.; Rodriguez, B.; Zasadzinski, J. *Science* **1989**, *245*, 1371.
- (3) Fogden, A.; Ninham, B. W. *Adv. Colloid Interface Sci.* **1999**, *83*, 85.
- (4) Dubois, M.; Gulik, Th.; Demé, B.; Zemb, Th. *C. R. Acad. Sci.* **1998**, *t. 1, Ser. IIC*, 567.
- (5) Dubois, M.; Belloni, L.; Zemb, Th.; Demé, B.; Gulik-Krzywicki, Th. *Prog. Colloid Polym. Sci.* **2000**, *115*, 238.
- (6) Jokela, P.; Joensson, B.; Khan, A. *J. Phys. Chem.* **1987**, *91*, 3291.
- (7) Jokela, P.; Joensson, B.; Eichmüller, B.; Fontell, K. *Langmuir* **1988**, *4*, 187.
- (8) Jokela, P.; Joensson, B. *J. Phys. Chem.* **1988**, *92*, 1923.
- (9) Joensson, B.; Jokela, P.; Khan, A.; Lindman, B.; Sadaghiani, A. *Langmuir* **1991**, *7*, 889.
- (10) Dubois, M.; Dedieu, J. C.; Demé, B.; Gulik-Krzywicki, Th.; Zemb, Th. *Chemistry in confined media*; Manne, S., Warr, G., Eds.; American Chemical Society: Washington, DC, 1999; pp 86–101.
- (11) Brasher, L. L.; Herrington, K. L.; Kaler, E. W. *Langmuir* **1995**, *11*, 4267.
- (12) Helm, C. A.; Laxhuber, L.; Lösche, M.; Möhwald, H. *Colloid Polym. Sci.* **1996**, *264*, 46.
- (13) Cevc, G.; Watts, A.; Marsh, D. *Biochemistry* **1981**, *20*, 4955.
- (14) Cevc, G. *Biochemistry* **1987**, *26*, 6305.
- (15) Marques, E.; Khan, A.; Lindman, B. *Thermochim. Acta* **2002**, *394*, 31.
- (16) Vautrin, C.; Dubois, M.; Zemb, Th. Rapport CEA-R-5984; CEA Saclay: Gif-sur-Yvette, France, 2001.
- (17) Vautrin, C.; Dubois, M.; Zemb, Th.; Schmolzer, S.; Hoffmann, H.; Gradzielski, M. *Colloids Surf. A* **2003**, *217*, 165.
- (18) Dubois, M.; Demé, B.; Gulik-Krzywicki, Th.; Dedieu, J. C.; Vautrin, C.; Desert, S.; Perez, E.; Zemb, Th. *Nature* **2001**, *411*, 672.
- (19) Plotnikov, V.; Brandts, J.; Lin, L.; Brandts, J. *Anal. Biochem.* **1997**, *250*, 237.
- (20) *Neutron, X-rays and light*; Lindner, P., Zemb, Th., Eds.; Elsevier: New York, 2002.
- (21) Piper, S. H. *J. Chem. Soc.* **1929**, 234.
- (22) Lynch, M. L. *Curr. Opin. Colloid Interface Sci.* **1997**, *2*, 495.
- (23) Cevc, G. *Phospholipids Handbook*; Marcel Dekker: New York, 1993.
- (24) Korlach, J.; Schwille, P.; Webb, W.; Feigenson, G. *Proc. Natl. Acad. Sci. U.S.A.* **1999**, *96*, 8461.
- (25) Bagatolli, L.; Gratton, E. *Biophys. J.* **1999**, *77*, 2090.
- (26) Radlinska, E.; Ninham, B.; Dalbiez, J. P.; Zemb, Th. *Colloids Surf.* **1990**, *46*, 213.
- (27) Sugar, I.; Thompson, Th.; Biltonen, R. *Biophys. J.* **1999**, *76*, 2099.
- (28) Johann, C.; Garidel, P.; Mennicke, L.; Blume, A. *Biophys. J.* **1996**, *71*, 3215.
- (29) Dörfler, H. D.; Pietschmann, N. *Colloid Polym. Sci.* **1990**, *268*, 559.
- (30) Vautrin, C.; et al. Manuscript in preparation.
- (31) Mantsch, H.; Weng, S.; Yang, P.; Eysel, H. *J. Mol. Struct.* **1994**, *324*, 133.
- (32) Schneider, M. F.; Marsh, D.; Jahn, W.; Kloesgen, B.; Heimburg, Th. *Proc. Natl. Acad. Sci. U.S.A.* **1999**, *96*, 14312.
- (33) Heimburg, Th. *Biochim. Biophys. Acta* **1998**, *1415*, 147.
- (34) Zemb, Th. *Colloids Surf. A* **1997**, *129–130*, 435–454.
- (35) Heimburg, Th. *Biophys. J.* **2000**, *78*, 1154.
- (36) Riske, K.; Amaral, L.; Lamy-Freund, M. *Biochim. Biophys. Acta* **2001**, *1511*, 297.
- (37) Riske, K.; Doebereiner, H.; Lamy-Freund, M. *J. Phys. Chem. B* **2002**, *106*, 239.
- (38) Riske, K.; Doebereiner, H.; Lamy-Freund, M. *J. Phys. Chem. B* **2003**, *107*, 5391.
- (39) Kosterlitz, J.; Thouless, D. *J. Phys. C* **1973**, *6*, 1181.
- (40) Barnes, I.; Derian, P.; Hyde, S.; Ninham, B.; Zemb, Th. *J. Phys.* **1990**, *51*, 2605.
- (41) Ravey, J.; Stebe, M.; Sauvage, M. *Colloids Surf. A* **1994**, *91*, 237.